A Study of the Interaction Between Implanted Pacemakers and the Radio-Frequency Field Produced by Magnetic Resonance Imaging Apparatus

Stefano Pisa, *Member, IEEE*, Giovanni Calcagnini, Marta Cavagnaro, *Member, IEEE*, Emanuele Piuzzi, Eugenio Mattei, and Paolo Bernardi, *Life Fellow, IEEE*

***Abstract*—Specific absorption rate (SAR) and temperature increases produced inside a thorax model by an MRI apparatus equipped with a birdcage antenna operating at 64 MHz have been studied both experimentally and numerically. Considering a pacemaker (PM) equipped with a unipolar catheter inserted inside the thorax model, peak SARs averaged over 1 mg between 240 and 6400 W/kg, depending on the catheter section and length, on its position inside the phantom, and on field polarization have been obtained close to the catheter tip. On the other hand, the average SAR in the whole thorax is not influenced by the presence of the PM. Temperature increments from 0.6 °C to 15 °C have been obtained for 6-min MRI investigations with the lowest values when the radio-frequency (RF) magnetic field is linearly polarized along a direction perpendicular to the implant plane.**

***Index Terms*—Cardiac pacemakers, dosimetry, magnetic resonance imaging (MRI), temperature.**

I. Introduction

MAGNETIC resonance imaging (MRI) is a tomography technique that measures the radio-frequency (RF) field produced by the magnetic moments of hydrogen nuclei during their precession following the application of RF pulses superimposed to a static magnetic field.

MRI is a widely accepted tool for the diagnosis of a variety of diseases. Nowadays, however, MRI is contraindicated for patients implanted with pacemakers (PMs) and implantable cardioverter defibrillators (ICDs) [1]–[3]. Potential effects of MRI on PMs, ICDs, and other active implantable medical devices include force and torque effects on the PM [4], undefined reed-switch state [5], and potential risk of heart stimulation and inappropriate pacing [6]. However, the most adverse effect seems to be the heating of the heart tissue around the catheter tip produced by the high currents induced on the catheter by the RF field used in MRI technique [7]–[10]. The amount of heating has been investigated in several studies on phantoms, and observed temperature elevations spread from not significant values up to tens of degrees. For example, Achenbach *et al*. [7] reported a temperature increase of 63.1 °C for a particular PM lead, Sommer *et al*. [8] obtained temperature increaseranging from 0.1 °C to 23.5 °C, depending on the electrode type, while in [9] and [10], a maximum temperature increase of about 6 °C has been found.

Manuscript received January 17, 2007; revised June 28, 2007.

S. Pisa, M. Cavagnaro, E. Piuzzi, and P. Bernardi are with the Department of Electronic Engineering, Sapienza University of Rome, Rome 00184, Italy (e-mail: pisa@die.uniroma1.it; cavagnaro@die.uniroma1.it; piuzzi@die.uniroma1.it; bernardi@die.uniroma1.it).

G. Calcagnini and E. Mattei are with the Italian National Institute of Health, Rome 00161, Italy (e-mail: giovanni.calcagnini@iss.it; eugenio.mattei@iss.it).

Digital Object Identifier 10.1109/TEMC.2007.915282

In orderto avoid thermal hazards, international agencies have issued guidelines reporting recommended limits. The International Commission on Non-Ionizing Radiation Protection (ICNIRP) [11] considers that, for whole-body exposures to MRI apparatus, no adverse health effects are expected if the increase in body core temperature does not exceed 1 °C. With regard to localized heating, ICNIRP assumes that adverse effects are avoided with a reasonable certainty if temperature remains lower than 38 °C in localized regions of the head, lower than 39 °C in the trunk, and less than 40 °C in the limbs. Consequently, in [11], limitations have been reported with reference to whole-body Specific absorption rate (SAR) (SAR_{WB}) and local SAR as averaged over 10 g of tissue (SAR_{10}). In particular, in normal conditions, the SAR_{WB} should not exceed 2 W/kg, while SAR_{10} is limited to 20 W/kg in the extremities and 10 W/kg in the head and trunk; however, care should be taken to ensure that the temperature rise is limited to 1 °C in the eye.

It must be noted that the temperatures considered safe in [11] are very conservative with reference to the heart. In fact, literature data on cardiac ablation indicate the development of abnormal automaticity and irreversible loss of cellular excitability of cardiac tissue for temperatures greater than 45 °C and 50 °C, respectively [12].

The thermal studies available in the literature [7]–[10] evidence, as previously discussed, strong variations in temperature at the catheter tip in PM holders during MRI. The steady-state temperatures are often above ICNIRP recommended limits, and in some cases, above the threshold for the loss of cellular excitability [12]. The reported variability in peak temperatures can be ascribed to the differences in power radiated by the MRI antenna, the length and the geometric structure of the lead, and the implant location. Consequently, an accurate analysis of the coupling between the RF field and the catheter appears to be very important.

In this paper, the power absorption and the temperature elevations induced by an MRI apparatus in a homogeneous thorax model, where a PM with a monopolar catheter is implanted, will be studied both experimentally and numerically. In particular, the effect of field polarization and the influence of the catheter geometry and radius on SAR and temperature increments will be analyzed.

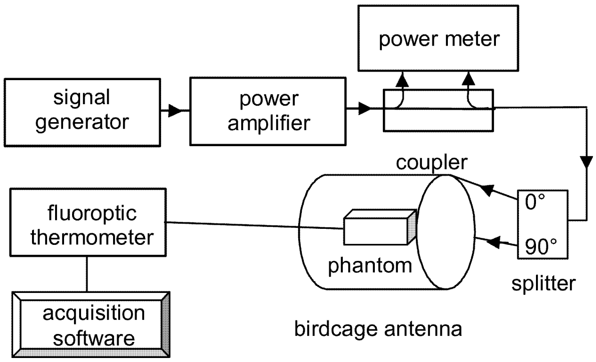

Fig. 1. Experimental setup.

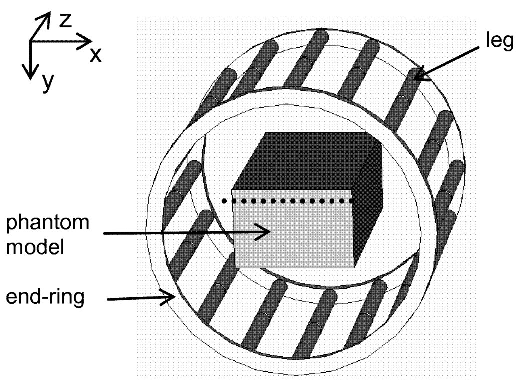

Fig. 2. Phantom model placed inside the birdcage antenna.

II. Methods

A. Experimental Setup

Experimental data have been provided by the Italian National Institute of Health. Fig. 1 shows the experimental setup. The 64-MHz signal is first amplified, and then, sent to the birdcage antenna through a power splitter with 90° output shift. The applied RF power is monitored with a power meter. The birdcage has an internal diameter of 62 cm, a height of 65 cm, and 16 legs (see Fig. 2).

The physical phantom is a parallelepiped box (30 cm × 20 cm × 60 cm) filled with gelled saline material (HEC 2%, NaCl 0.36%) that mimics the electrical and thermal properties of an average human tissue at the considered frequency [13]. The measured permittivity and conductivity values of the gelled material are equal to 78.2 and 0.6 S/m, respectively [14]. A tissue density (ρ) of 1006 kg/m^3, together with a thermal conductivity (K) equal to 0.2 W/(m $\cdot ^\circ$ C) and a specific heat (C) of 4178 J/(kg $\cdot$ °C) have been provided by the HEC manufacturer [15].

A unipolar PM with a 60-cm-long catheter (see Fig. 3), which represents the usual length for commercial catheters, is fixed to a plastic grid and immersed in the phantom at a depth of 1 cm inside the saline material.

Temperature increments are monitored via a four-probe Luxtron 3100 fluoroptic$^{\mathrm{TM}}$ thermometer equipped with SMM probes accurate to 0.1 °C at the point of calibration (21 °C in our case). SAR (in watts per kilogram) values are extrapolated

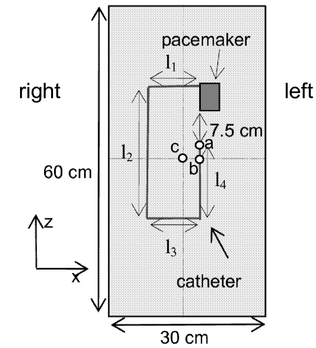

Fig. 3. Section of the phantom model 1 cm below the phantom surface (dotted line in Fig. 2) showing the geometry of PM and catheter.

from initial temperature rise rate through the equation

$$\mathrm{SAR} = C \left.\frac{dT}{dt}\right|_{t=0}. \qquad (1)$$

In order to reduce the thermal diffusion influence on SAR determination, the temperature variation is computed between 3 and 10 s from the beginning of the exposure.

B. Electromagnetic Model

Numerical simulations have been performed using a code based on a conformal finite-difference time-domain (FDTD) scheme [16] with graded mesh (C-GM-FDTD) [17], [18]. The investigated region has been divided in cells of variable size, from 1 to 10 mm (with the smaller cells in the catheter region), and the different structures (metallic birdcage, dielectric phantom, and metallic PM and catheter) have been modeled, assigning to each cell an equivalent permittivity and conductivity evaluated as the weighted fraction of the materials contained in the cell, according to the conformal scheme described in [16]. The FDTD domain has been closed with uniaxial perfectly matched layer (UPML) boundary conditions (four cells, 0.01% reflection, parabolic profile) [19].

A current excitation with sinusoidal time behavior has been imposed at the center of the birdcage legs. A phase delay equal to the azimuthal angle, corresponding to an increasing 22.5° phase shift between elements, has been applied to produce a left circular magnetic polarization with respect to the positive z-axis. This polarization is necessary for having the maximum coupling between the RF field and the nuclear proton spin [20]. Linear polarizations can also be applied with a birdcage antenna. These are simulated by imposing current excitations with the same phase but with amplitudes varying cosinusoidally or sinusoidally with the azimuthal angle in order to obtain a y-directed or an x-directed magnetic field linear polarization, respectively [21]. However, it must be noted that a linear polarization can be divided in the sum of a left and a right circular polarization. Hence, to achieve, in this case, a circularly polarized magnetic field component having a magnitude equal to that obtained for the previously considered excitation, the power to be sent to the birdcage should be doubled [21].

Once the steady-state conditions are reached and the amplitude of the three electric field components are determined in the center of each cell inside the phanthom, the SAR is evaluated as

$$\mathrm{SAR}(i,j,k) = \frac{\sigma(i,j,k)\left[E_x^2(i,j,k)+E_y^2(i,j,k)+E_z^2(i,j,k)\right]}{2\rho(i,j,k)} \quad (2)$$

where $\sigma(i,j,k)$ and $\rho(i,j,k)$ are the conductivity and the density of the tissue filling the $(i,\,j,\,k)$ cell. The considered values are the SAR averaged over 1 mg ($\approx$ 1 mm^3), which is the quantity usually measured in experimental studies, its peak value inside the thorax ($\mathrm{SAR_{PEAK}}$), and the average over the whole thorax ($\mathrm{SAR_{WB}}$) that quantifies the total power absorption.

C. Thermal Model

The temperature distribution $T = T(\mathbf{r},t)$ has been simulated by solving Fourier's heat transfer equation (FHE) [22] inside the phantom

$$\nabla\cdot(K(\mathbf{r})\nabla T) + Q_v(\mathbf{r}) \;= C(\mathbf{r})\rho(\mathbf{r})\frac{\partial T}{\partial t} \qquad (\mathrm{W/m^3}). \quad (3)$$

The two terms on the left-hand side of (3) represent the heat transfer through internal conduction, and the electromagnetic power deposition [Q_v (in watts per cubic meter)]. These terms are equated with the temperature increase (or decrease) per unit time multiplied by the thermal capacitance of 1 m^3 of tissue (right-hand side). The thermal capacitance is given by the product between the tissue-specific heat and the density. The aforementioned FHE, in order to be solved, must be completed by an appropriate boundary condition, able to model heat exchange from the phantom surface to the external environment. This boundary condition is obtained by imposing the continuity of the heat flow perpendicular to the phantom surface, and can be expressed as [22]

$$-K(\mathbf{r})\left(\nabla T\cdot \boldsymbol{n}_0\right)_S \;= H\left(T_S - T_A\right) \qquad (\mathrm{W/m^2}) \quad (4)$$

where S is the phantom surface and $\boldsymbol{n}_0$ is the unit vector normal to S. The term on the right-hand side of (4) models heat losses due to convection and radiation, proportional to the difference between temperature of the phantom surface (T_S) and external temperature (T_A) through the parameter H (in watts per square meter per degree celsius). A convection coefficient equal to 10 $\mathrm{W/(m^2 \cdot {}^\circ C)}$ and an external temperature T_A equal to 21 °C have been assumed in all the simulations. To obtain a finite-difference formulation of the FHE and boundary condition, the phantom is divided in cubic cells of 1 mm side, and the temperature is evaluated in a grid of points defined at the centers of the cells. Equation (3) is then solved by using an alternate direction implicit finite difference (ADI-FD) formulation [23].

III. Results

A. Thorax Exposure Without the Pacemaker

At first, the exposure of the thorax phantom without the PM has been studied both experimentally and numerically.

During the experiments, the birdcage antenna operates at 64 MHz with a radiated power of 100 W that is close to the average power delivered by the MRI apparatus during a typical sequence for imaging acquisition. Calorimetric measurements performed on the exposed phantom revealed that the $\mathrm{SAR_{WB}}$ is equal to about 1 W/kg.

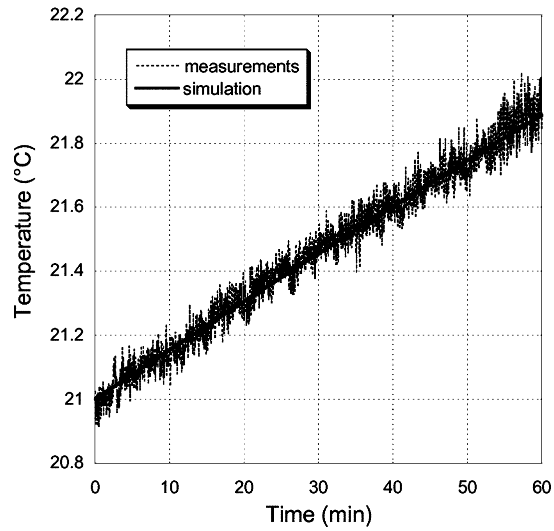

Fig. 4. Time behavior of the temperature in the physical and simulated phantoms (without PM) evaluated at point "c" in Fig. 3.

The same exposure has been simulated by using the C-GM-FDTD code for the solution of the EM problem and the ADI-FD code for the solution of Fourier's equation. Due to the differences between the birdcage field excitation in the experimental setup and in the numerical simulations, and in order to compare the results, the current excitation amplitudes in simulations have been chosen to give rise in the thorax model to a $\mathrm{SAR_{WB}}$ of 1 W/kg equal to the experimental data. The considered current excitation produces, in the absence of the thorax, magnetic field magnitudes of about 2.5 A/m in the birdcage central region that are close to the typical mean field value adopted in the fast spin echo sequences used in MRI [20].

Fig. 4 shows the measured (continuous line) and simulated (dashed line) temperature in the phantom in a point 1 cm below the phantom surface (point "c" in Fig. 3). A temperature increase of about 0.9 °C after 60 min of exposure can be observed. The linear behavior is due to the fact that, for the considered problem, and by considering a penetration depth (δ) of 0.1 m, a time constant equal to $\tau = C\rho\,\delta^2/K \approx 3000$ min is expected [24].

The performed numerical simulation allows us to analyze the field and SAR distributions inside the phantom. Fig. 5(a) shows the obtained electric field z-component on a coronal plane (x–z in Fig. 2) 1 cm below the thorax surface (corresponding to the dotted line section of Fig. 2 where the PM and the catheter will be placed). The figure shows that the induced electric field presents a z-component with the highest values close to the left and right box faces. The electric field x-component (not shown) has lower values (< 30 V/m) with maxima close to the top and bottom faces. Finally, the electric field y-component (not shown) is always lower than 10 V/m. The SAR distribution is shown in Fig. 5(b) for the same coronal plane of Fig. 5(a). From the figure, it can be noted that this distribution is very similar to that of the electric field z-component, reported in Fig. 5(a). In

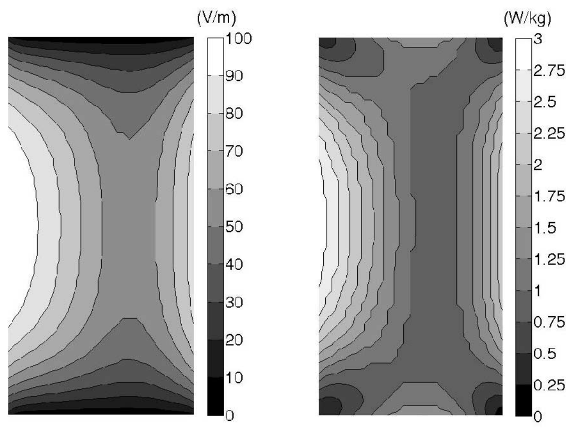

(a) (b)

Fig. 5. (a) E_z field distribution on a coronal plane (*x–z* in Fig. 2) 1 cm below the phantom surface for a left circular polarization. (b) SAR distribution on the same section.

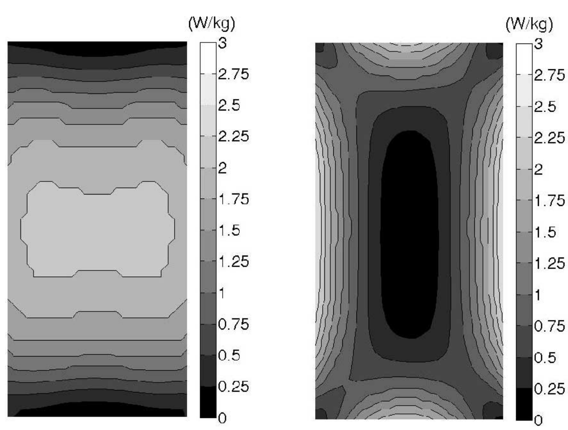

(a) (b)

Fig. 6. SAR distribution in the coronal section, 1 cm below the phantom surface, for magnetic field linear polarizations. (a) *x*-directed. (b) *y*-directed.

fact, this is the strongest electric field component, and the thorax model is homogeneous. Under these conditions, a SAR_{PEAK} of 3.1 W/kg has been computed, and as stated before, SAR_{WB} is equal to 1.0 W/kg. It is worth noting that both the SAR and the field distribution do not show horizontal symmetry. In fact, while the structure is symmetric, the field excitation presents an azimuthal phase shift that gives rise to higher values on the right side of the phantom model.

The same structure has been studied by applying *x*-directed and *y*-directed magnetic field linear polarizations. Fig. 6 shows the obtained SAR distributions in the same plane of Fig. 5 with a current excitation settled to achieve a SAR_{WB} of 1 W/kg. Both the *x*-directed [see Fig. 6(a)] and the *y*-directed [see Fig. 6(b)] linear polarizations give rise to a symmetric distribution, with respect to the *x*- and *z*-axes, and to a SAR_{PEAK} of about 2.7 W/kg slightly lower than the circular polarization case. However, as discussed in Section II-B, the power to be sent to the birdcage must be doubled, thus doubling SAR values [20]. The electric field simulation results (not reported) show that, as for the circular polarization case, the SAR distribution for linear polarization follows quite well that of the electric field *z*-component.

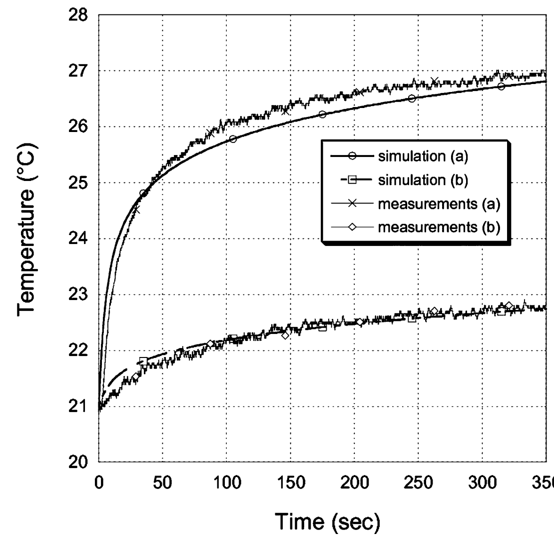

Fig. 7. Time behavior of the temperature on the physical and simulated phantoms (with PM) at the catheter tip (point “a” in Fig. 3) and 2 cm below the catheter tip (point “b” in Fig. 3).

B. Effect of the Pacemaker Geometry and Position

The exposure to a power of 100 W at 64 MHz of the thorax model in the presence of a PM with a unipolar catheter has then been studied both experimentally and numerically.

In the experiments, a commercial PM with a 60-cm-long catheter ($l_1 = 10$ cm, $l_2 = 26$ cm, $l_3 = 10$ cm, $l_4 = 14$ cm in Fig. 3) has been placed inside the thorax. The PM is located in the left side in a typical operating position with the catheter tip 7.5 cm from the PM.

The same exposure has been simulated by using the C-GM-FDTD code for the solution of the EM problem and the ADI-FD code for the solution of Fourier’s equation. In the EM simulations, the PM has been modeled as a copper box (40 mm $\times$ 10 mm $\times$ 50 mm) and the 60-cm-long catheter has been modeled as a cylindrical wire of copper with a radius of 0.4 mm with the same rectangular geometry considered in the experiments (see Fig. 3). The same birdcage current excitation applied in the absence of the PM has been adopted.

Fig. 7 shows the time behavior of the measured and simulated temperature. After 6 min exposure, a temperature increment of 6 °C at a point just above the catheter tip (a in Fig. 3) and 1.8 °C at a point 2 cm below the catheter tip (b in Fig. 3) can be observed, with a good agreement between measurements and simulations.

Further numerical simulations have been performed in order to analyze the SAR distributions inside the phantom and the currents along the catheter for circular and linear excitations.

Fig. 8 shows the obtained SAR distributions in the coronal section passing through the catheter. Note that the grayscale is strongly saturated; in fact, the presence of the catheter determines high local SAR values.

SAR_{PEAK} of 2400, 6400, and 250 W/kg have been obtained at the catheter tip for the circular, *x*-directed and *y*-directed linear polarizations, respectively. SAR_{WB} is about 1.0 W/kg in all cases. Temperature simulations showed temperature increments at the catheter tip of 6 °C, 15 °C, and 0.6 °C after 6 min of exposure, for the three considered cases.

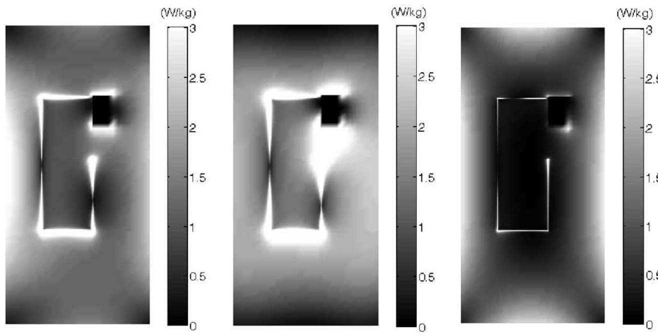

(a) (b) (c)

Fig. 8. SAR distributions in the coronal section passing through the catheter (see Fig. 2). (a) Left circular polarization. (b) Linear x-directed. (c) Linear y-directed polarizations.

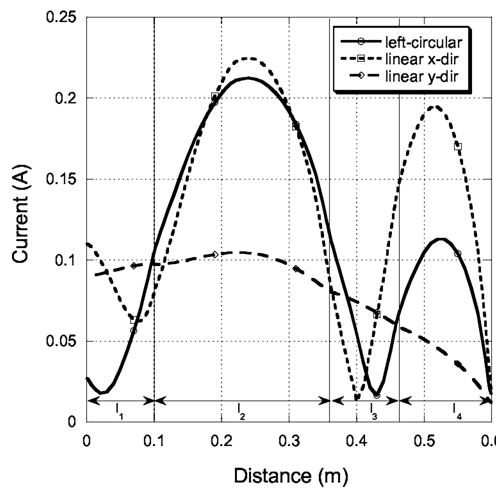

Fig. 9. Current distribution along the catheter for clockwise and linear excitations (pacemaker on the left of the thorax).

The current distribution along the catheter has been computed as the circulation of the magnetic field around the catheter axis. Fig. 9 shows the current distributions obtained for the three considered cases. The distance along the wire from the point in which the catheter is inserted in the PM is reported on the horizontal axis (the catheter length is 60 cm). The obtained current distributions can be explained observing that, at 64 MHz and in the presence of the dielectric phantom, the wavelength is about 50 cm, and hence, comparable with the catheter length. Moreover, in quasi-static conditions, the current inside the wire is mainly produced by the electric field component, obtained in the absence of the wire (unperturbed field), parallel to the wire axis. Correspondingly, in the considered exposure condition, the strongest currents are produced by the E_z-field along the l_2 and l_4 segments while lower currents are produced by the lower E_x component, acting on l_1 and l_3.

The comparison between the SAR distributions reported in Fig. 8 and the current distributions in Fig. 9 evidences that the current along the wire follows an opposite behavior with respect to the SAR distribution around the wire. In fact, the presence of the wire strongly alters the field distribution as compared to the one obtained without the catheter. Therefore, the SAR

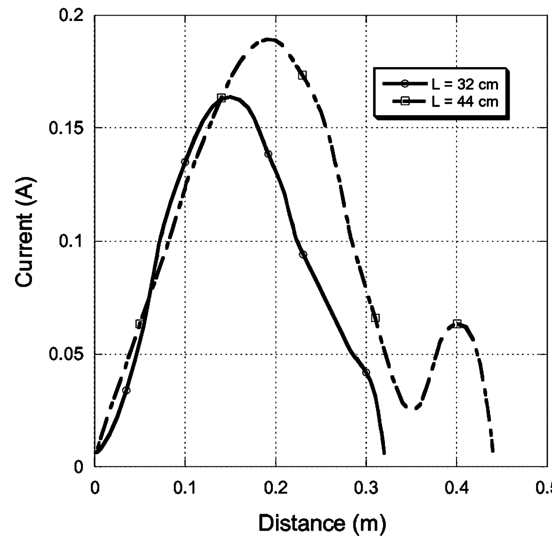

Fig. 10. Current distribution along the catheter for clockwise excitations and catheters of different lengths.

(and hence, the electric field) decreases close to the wire section where the current grows and *vice versa*. For example, the current presents a maximum at the center of the l_2 and l_4 segments where the SAR has a minimum [darker regions in Fig. 8(a)].

A further study has been performed in order to investigate the effect of the catheter cross section on SAR. To this end, two more wires of radius 0.2 and 0.8 mm, respectively, have been considered. The simulation results for a circularly polarized magnetic field have evidenced that the SAR values at the catheter tip increase when the wire section reduces. $\mathrm{SAR}_{\mathrm{PEAK}}$ values of 2500 and 76 W/kg have been obtained for wire radii of 0.2 and 0.8 mm, respectively. It is worth noting that the increase of the wire radius determines an increase of the current along the wire and at the tip. However, the corresponding increase of the section produces a reduction of the current density, and hence, the final effect is a reduction of the SAR at the catheter tip.

The effect of the catheter length has also been investigated by considering catheters with a 0.4-mm radius and different lengths. In the considered simulations, the distance between the catheter tip and the PM has been maintained to 7.5 cm, while the length of the catheter has been changed. Fig. 10 shows the results obtained for a total length of 32 cm ($l_1 = 7\,\mathrm{cm}$, $l_2 = 15\,\mathrm{cm}$, $l_3 = 7\,\mathrm{cm}$, and $l_4 = 3\,\mathrm{cm}$) and for a total length of 44 cm ($l_1 = 10\,\mathrm{cm}$, $l_2 = 18\,\mathrm{cm}$, $l_3 = 10\,\mathrm{cm}$, and $l_4 = 6\,\mathrm{cm}$). In these simulations, $\mathrm{SAR}_{\mathrm{PEAK}}$ of 1000 and 1400 W/kg have been obtained for the two considered lengths.

In the previous analysis, the PM was implanted in the left part of the thorax. However, in clinical practice, the PM can also be implanted on the right part of the thorax. Numerical simulations have been performed in order to study this exposure condition and by considering both circular and linear polarizations. Fig. 11 shows, for the circular polarization case, the SAR distribution in the coronal section passing through the catheter. $\mathrm{SAR}_{\mathrm{PEAK}}$ is always localized at the catheter tip and a value of about 4500 W/kg has been obtained. Moreover, $\mathrm{SAR}_{\mathrm{PEAK}}$ values of 6400 and 240 W/kg have been obtained for the linear x-directed and y-directed polarizations, respectively. These last

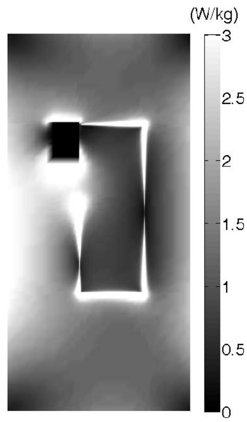

Fig. 11. SAR distribution in the coronal section passing through the catheter (see Fig. 2) for left circular polarization. Catheter in the right part of the thorax.

values are practically identical to those obtained for the left PM placement, while, in the circular polarization case, higher values are obtained with respect to the left placement. This is due to the asymmetry of the E_z-field distribution [see Fig 5(a)] with highest field values on the right part of the thorax where the catheter tip is placed in this last exposure condition.

IV. Conclusion

The SAR induced by an MRI apparatus in a thorax model with an implanted PM equipped with a monopolar catheter has been studied considering different implant geometries and field polarizations.

The study has been limited only to a simple homogeneous phantom because the main aim was to compare numerical results with experimental measurements in order to validate the proposed numerical methodology and to study the effect of catheter geometry and field polarization.

The performed study has evidenced the following.

1) The region with the highest SAR values is the one around the catheter tip where the current flowing along the catheter wire can induce strong current densities in the tissues.
2) The currents along the catheter are mainly induced by the electric field parallel to the catheter axis. Since strong E-field z-components are present, the highest currents are induced along z-directed wires.
3) Generally, short catheters with short vertical wires give rise to lower SAR at the catheter tip. However, the lowest SAR_{PEAK} values have been obtained when the magnetic field is linearly polarized on a direction perpendicular to the implant plane (y direction in Fig. 3).
4) The SAR_{PEAK} values obtained for the considered exposure condition give rise to temperature increments at the catheter tip ranging between 0.6 °C and 15 °C.

It is important to remember that, on the basis of ICNIRP recommendation, no adverse health effects are expected if the temperature in localized parts of the trunk does not exceed 39 °C [11]. On the basis of the present study, these limits can be reached for a PM located in a simple homogeneous parallelepiped phantom. However, reductions in peak temperatures are expected if an anatomical body model with a catheter following the vein path is considered together with the presence of blood perfusion and thermoregulation. In fact, the insertion of the PM in an anatomical model brings part of the catheter to be placed more deeply inside the body in regions with lower electric fields, and the presence of perfusion and thermoregulation surely reduces the temperature increment also if the percentage of reduction is not predictable due to the complexity of the problem (geometry, thermal parameters, etc.). The adopted techniques, with the inclusion of blood perfusion and thermoregulation in the thermal model [25], will be applied to anatomically accurate body phantoms (e.g., Visible Human [26]) in a future work. The consideration of this anatomical model will make it possible to investigate if, under realistic conditions, the use of particular field polarizations, implant arrangements, or any design technique able to reduce the current along the wire can prevent temperature increases from exceeding the levels considered safe by ICNIRP, thus allowing MRI to PM holders.

References

[1] J. R. Gimbel and E. Kanal, “Can patients with implantable pacemakers safely undergo magnetic resonance imaging?,” *J. Amer. Coll. Cardiol.*, vol. 43, no. 7, pp. 1325–1327, Apr. 2004.

[2] E. Kanal and F. G. Shellock, “Policies, guidelines, and recommendations for MR imaging sagety and patient management. SMRI Safety Committee,” *J. Magn. Reson. Imag.*, vol. 2, no. 2, pp. 247–248, Mar./Apr. 1992.

[3] F. G. Shellock, *Magnetic Resonance: Health Effects and Safety*. Boca Raton, FL: CRC, 2001.

[4] R. Luechinger, F. Duru, M. B. Scheidegger, P. Boesiger, and R. Candinas, “Force and torque effects of a 1.5-tesla MRI scanner on cardiac pacemakers and ICDs,” *Pacing Clin. Electrophysiol.*, vol. 24, no. 2, pp. 199–205, Feb. 2001.

[5] R. Luechinger, F. Duru, V. A. Zeijlemaker, M. B. Scheidegger, P. Boesiger, and R. Candinas, “Pacemaker reed switch behavior in 0.5, 1.5, and 3.0 tesla magnetic resonance imaging units: Are reed switches always closed in strong magnetic fields?,” *Pacing Clin. Electrophysiol.*, vol. 25, no. 10, pp. 1419–1423, Oct. 2002.

[6] J. A. Erlebacher, P. T. Cahill, F. Pannizzo, and R. J. Knowles, “Effect of magnetic resonance imaging on DDD pacemakers,” *Amer. J. Cardiol.*, vol. 57, no. 6, pp. 437–440, Feb. 1986.

[7] S. Achenbach, B. Moshage, W. Diem, T. Bieberle, V. Schibgilla, and K. Bachmann, “Effects of magnetic resonance imaging on cardiac pacemakers and electrodes,” *Amer. Heart. J.*, vol. 134, no. 3, pp. 467–473, Sep. 1997.

[8] T. Sommer, C. Vahlhaus, G. Lauck, A. von Smekal, M. Reinke, U. Hofer, W. Bloch, F. Traber, C. Schneider, J. Gieseke, W. Jung, and H. Schild, “MR imaging and cardiac pacemaker: In-vitro evaluation and in-vivo studies in 51 patients at 0.5 T,” *Radiology*, vol. 215, no. 3, pp. 869–879, Jun. 2000.

[9] A. Roguin, M. M. Zviman, G. R. Meininger, E. R. Rodrigues, T. M. Dickfeld, D. A. Bluemke, A. Lardo, R. D. Berger, H. Calkins, and H. R. Halperin, “Modern pacemaker and implantable cardioverter/defibrillator systems can be magnetic resonance imaging safe. In vitro and in vivo assessment of safety and function at 1.5 T,” *Circulation*, vol. 110, no. 5, pp. 475–482, May 2004.

[10] S. Pisa, G. Calcagnini, M. Cavagnaro, E. Piuzzi, M. Triventi, and P. Bernardi, “SAR and temperature elevations in pacemaker holders exposed to EM fields produced by MRI apparatus,” in *Proc. 2006 IEEE MTT-S Int. Microw. Symp. Dig.*, San Francisco, CA, pp. 1754–1757.

[11] ICNIRP Statement, “Medical magnetic resonance (MR) procedures: Protection of patients,” *Health Phys.*, vol. 87, no. 2, pp. 197–216, Aug. 2004.

[12] S. Nath, C. Lynch, J. G. Whayne, and D. E. Haines, “Cellular electrophysiological effects of hyperthermia on isolated guinea pig papillary muscle. Implications for catheter ablation,” *Circulation*, vol. 88, pp. 1826–1831, Oct. 1993.

[13] ASTM Designation: F2182-02a, *Standard test method for measurement of radio frequency induced heating near passive implants during magnetic resonance imaging*. West Conshohocken, PA, ASTM International, 2002.

[14] T. W. Athey, M. A. Stuckly, and S. S. Stuckly, "Measurement of RF permittivity of biological tissues with an open-ended coaxial line: Part I," *IEEE Trans. Micow. Theory Tech.*, vol. MTT-30, no. 1, pp. 82–86, Jan. 1982.
[15] Aqualon, *Natrosol Hydroxyethylcellulose: A Nonionic Water Soluble Polymer, Physical and Chemical Properties,* Aqualon, Hercules Inc., Wilmington, DE, 1987.
[16] D. Caratelli and R. Cicchetti, "A full-wave analysis of interdigital capacitor for planar integrated circuits," *IEEE Trans. Magn.*, vol. 39, no. 3, pp. 1598–1601, May 2003.
[17] M. Yang and Y. Chen, "Automesh: An automatically adjustable, nonuniform, orthogonal FDTD mesh generator," *IEEE Antennas Propag. Mag.*, vol. 41, no. 2, pp. 13–19, Apr. 1999.
[18] S. Pisa, M. Cavagnaro, E. Piuzzi, and V. Lopresto, "Numerical-experimental validation of a GM-FDTD code for the study of cellular phones," *Microw. Opt. Technol. Lett.*, vol. 47, no. 4, pp. 396–400, Nov. 2005.
[19] A. Taflove and S. C. Hagness, *Computational Electrodynamics: The Finite-Difference Time-Domain Method*. Boston, MA: Artech House, 2000.
[20] U. D. Nguyen, S. Brown, I. A. Chang, J. K. Krycia, and M. S. Mirotznik, "Numerical evaluation of heating of the human head due to magnetic resonance imaging," *IEEE Trans. Biomed. Eng.*, vol. 51, no. 8, pp. 1301–1309, Aug. 2004.
[21] C. M. Collins, S. Li, and M. B. Smith, "SAR and B1 field distributions in a heterogeneous human head model within a birdcage coil," *Magn. Res. Med.*, vol. 40, pp. 847–856, 1998.
[22] N. Ozisik, *Heat Transfer: A Basic Approach*. New York: McGraw-Hill, 1985.
[23] S. Pisa, M. Cavagnaro, E. Piuzzi, P. Bernardi, and J. C. Lin, "Power density and temperature distributions produced by interstitial arrays of sleeved-slot antennas for hyperthermic cancer therapy," *IEEE Trans. Microw. Theory Tech.*, vol. 51, no. 12, pp. 2418–2426, Dec. 2003.
[24] K. R. Foster, A. Lozano-Nieto, and P. R. Riu, "Heating of tissues by microwaves: A model analysis," *Bioelectromagnetics*, vol. 19, pp. 420–428, 1998.
[25] P. Bernardi, M. Cavagnaro, S. Pisa, and E. Piuzzi, "Specific absorption rate and temperature elevation in a subject exposed in the far-field of radio-frequency sources operating in the 10–900 MHz range," *IEEE Trans. Biomed. Eng.*, vol. 50, no. 3, pp. 295–304, Mar. 2003.
[26] P. A. Mason, W. D. Hurt, T. J. Walters, J. A. D'Andrea, P. Gajsek, K. L. Ryan, D. A. Nelson, K. I. Smith, and J. M. Ziriax, "Effects of frequency, permittivity, and voxel size on predicted specific absorption rate values in biological tissue during electromagnetic-field exposure," *IEEE Trans. Microw. Theory Tech.*, vol. 48, no. 11, pp. 2050–2058, Nov. 2000.

Stefano Pisa (M'91) was born in Rome, Italy, in 1957. He received the M.S. degree (*cum-laude*) and the Ph.D. degree both in electronic engineering from the University of Rome "La Sapienza," Rome, Italy, in 1985 and 1988, respectively.

In 1989, he joined the Department of Electronic Engineering, University of Rome "La Sapienza," in 1989, as a Researcher, and in 2001, became an Associate Professor. His current research interests include the interaction between electromagnetic fields and biological systems, therapeutic and diagnostic applications of electromagnetic fields, and the modeling and design of microwave circuits.

Dr. Pisa was a member of the Joint Working Group (JWG) 15 created by the International Electrotechnical Commission (IEC) from 1995 to 1999. From 1997 to 1999, he was the coordinator of a working package in the framework of the European project "cellular phones standard" (CEPHOS). From 1995 to 2002, he was a Secretary of the IEEE Microwave Theory and Techniques Society (MTT-S)/Antennas and Propagation Society (AP-S) Central and South Italy Section Joint Chapter. He was also an Editor of the disk of complete references 1993–1995 for the Commission K (Electromagnetics in Biology and Medicine) of the International Union of Radio Science (URSI). From 1995 to 1996, he was the coordinator of a "working package" of the Italian project on "wide-band wireless local area networks" (WWLANs) of the Italian National Research Council (CNR). He was a Coordinator of the activity "development and optimization of dedicated software for the evaluation of SAR in subjects exposed to mobile telecommunication systems" of the Italian National Project for 2001–2004, funded by the Ministry for Education, University, and Research, and devoted to the protection of people and environment from electromagnetic emissions.

Giovanni Calcagnini received the M.S. degree in electronic engineering, from the University of Rome "La Sapienza," Rome, Italy, in 1993, and the Ph.D. degree in biomedical engineering from the University of Bologna, Bologna, Italy, in 1997.

Since 1998, he has been with the Department of Technologies and Health, Italian National Institute for Health, Rome. His current research interests include the area of signal processing and electromagnetic interference with medical devices.

Marta Cavagnaro (M'01) was born in Rome, Italy, in 1966. She received the M.S. degree (*cum-laude*) and the Ph.D. degree both in electronic engineering from the University of Rome "La Sapienza," Rome, Italy, in 1993 and 1997, respectively.

Since 2000, she has been an Assistant Professor with the Department of Electronic Engineering, University of Rome "La Sapienza." Her current research interests include dosimetric aspects of the interaction between electromagnetic (EM) fields and biological systems, medical applications of EM fields (e.g., microwave ablation treatments), environmental impact of EM fields, and numerical techniques in electromagnetics.

Emanuele Piuzzi was born in Lecce, Italy, in 1972. He received the M.S. degree (*cum-laude*) and the Ph.D. degree both in electronic engineering from the University of Rome "La Sapienza," Rome, Italy, in 1997 and 2001, respectively.

He is currently an Assistant Professor in the Department of Electronic Engineering, Sapienza University of Rome, where he is engaged in teaching electrical measurements. His current research interests include the measurement of dielectric characteristics and levels of layered fluids through time-domain reflectometer and frequency-domain approaches, impedance pneumography and ultra-wideband radar techniques for the monitoring of cardiopulmonary activity in patients, interaction between electromagnetic fields radiated by mobile communication systems and exposed subjects, and the environmental impact reduction of cellular communication systems through the use of smart antennas for cellular base stations.

Dr. Piuzzi was one of the recipients of the 1999 International Union of Radio Science (URSI) Young Scientist Award.

Eugenio Mattei was born in Rome, Italy, in 1981. He received the Bachelor's degree in medical engineering, and the Master's degree from the University of Rome "Tor Vergata," Rome, Italy, in 2003 and 2005, respectively. He is currently working toward the Ph.D. degree in bioengineering at the University of Rome "La Sapienza," Rome.

Since 2003, he has been with Cardiovascular Bioengineering Department, Italian National Institute of Health, Rome. Since 2005, he has been engaged in the development of a numerical model for the analysis of thermal and nonthermal effects caused by MRI on pacemaker leads and its validation through experimental measures. His current research interests include the evaluation of the compatibility of medical devices with electromagnetic fields, therapeutic, and diagnostic applications of electromagnetic fields, and the modeling and design of electrical devices used in clinical environments.

Paolo Bernardi (M'66–SM'73–F'93–LF'01) was born in Civitavecchia, Italy, in 1936. He received the Electr. Eng. Laurea and Libera Docenza degrees from the University of Rome, Rome, Italy, in 1960 and 1968, respectively.

Since 1961, he has been with the Department of Electronics, University of Rome "La Sapienza," Rome, where he became a Full Professor in 1976, and then was the Head of the department from 1982 to 1988. His current research interests include the propagation of electromagnetic waves in ferrites, millimeter-wave components, biological effects of electromagnetic waves, and electromagnetic compatibility. He is the author or coauthor of more than 200 scientific papers and various invited presentations at international workshops and conferences. He was the Guest Editor of the special issues of the *Alta Frequenza* on "nonionizing electromagnetic radiation" for March 1980 and *Wireless Networks* "exposure hazards and health protection in personal communication services" for December 1997. He is currently a member of the Editorial Board for *Microwave and Optical Technology Letters*.

Dr. Bernardi is a member of the Bioelectromagnetics Society, the European Bioelectromagnetics Association, and "Socio Fedele" of the Italian Electrical and Electronic Society (AEI). From 1979 to 1980, he was the Chairman of the IEEE Middle and South Italy Section. He was the Chairman of the International Union of Radio Science (URSI) Commission K on Electromagnetics in Biology and Medicine for the triennium 1993–1996, the Vice Chairman of the European Community COST Project 244 on biomedical effects of electromagnetic radiation for 1993–1997, the Project Coordinator of the European Community Project CEPHOS for 1998–2000, which was devoted to electromagnetic dosimetry and compliance with standards of mobile cellular phones, and the Scientific Coordinator of the Italian National Project for 2001–2004, devoted to the protection of people and environment from electromagnetic emissions. He was the recipient of the IEEE Centennial Medal during the centennial year 1984. He was a member of the editorial board for the IEEE TRANSACTIONS ON MICROWAVE THEORY AND TECHNIQUES.